Journal of Materials and Environmental Science
ISSN : 2028-2508
e-ISSN : 2737-890X
CODEN : JMESCN

J. Mater. Environ. Sci., 2025, Volume 16, Issue 10, Page 1893-1907

http://www.jmaterenvironsci.com

Determination of the specific surface areas of activated carbons produced from local lignocellulosic biomass (Niger) using the BET, Langmuir and BJH methods

Ousmaila SANDA MAMANE [1,2], Rabilou SOULEY MOUSSA[2], Mahamane Nassirou AMADOU KIARI[2,3,4*], Abdoul Rachid CHAIBOU YACOUBA, Maâzou SIRAGI DOUNOUNOU BOUKARI[2], Ali SANDA BAWA[1,2], Ousmane MAHAMAN SANI[1,2], Maman Mousbahou MALAM ALMA[2], Ibrahim NATATOU[1,2]

[1]*National School of Engineering and Energy Sciences/ University of Agadez, Niger*
[2]*Department of Chemistry, Faculty of Science and Technology, Materials/ Water and Environment Laboratory/ Abdou Moumouni University, Niger*
[3]*Laboratory of Industrial Processes of Synthesis, the Environment and New Energies (LAPISEN), Institut National Polytechnique Félix Houphouët-Boigny, BP 1093, Yamoussoukro, Côte d'Ivoire*
[4]*African Center of Excellence for the Recovery of Waste into High Value-Added Products (CEA-VALOPRO), Yamoussoukro, Côte d'Ivoire*

Corresponding author, Email address: amadounassirou73@gmail.com

Received *01 Sept 2025,*
Revised *24 Sept 2025,*
Accepted *29 Sept 2025*

Keywords:
- ✓ *Biomass;*
- ✓ *Activated carbons;*
- ✓ *Specific surfaces;*
- ✓ *Isotherm;*
- ✓ *Nitrogen adsorption.*

Citation*: Sanda Mamane O., Souley Moussa R., Amadou Kiari M.N., Chaibou Yacouba A.R., Siragi Dounounou Boukari M., Sanda Bawa A., Mahaman Sani O., Malam Alma M.M., Natatou I. (2025) Determination of the specific surface areas of activated carbons produced from local lignocellulosic biomass (Niger) using the BET, Langmuir and BJH methods, J. Mater. Environ. Sci., 16(10), 1893-1907.*

Abstract: The aim of this work is to determine the Specific Surface Areas according to the Brunauer Emmet Teller (BET) model, the Langmuir model and the Barret Joyner Halenda (BJH) model of activated carbons produced from local biomasses (*Balanitès aegyptiaca* and *Hyphaene thebaica*). Analyses of the specific surfaces of Elaborated Activated Carbon were carried out using a brand-name instrument (MICROMERITICS Gemini VII Surface Area & Porosity) by liquid nitrogen adsorption at 77 K. Isotherms are obtained by plotting the quantity of N_2 adsorbed as a function of relative pressure $\frac{P}{P^0}$. Specific surface areas are determined using three models: BET, Langmuir and BJH. Specific surface areas are determined using three models, namely BET, Langmuir and BJH. Analysis of the results of this study shows that the isotherms are essentially type I for CA-BA-H_3PO_4-25%, CA-HT-H_3PO_4-25% and CA-HT-H_3PO_4-40%, mixed type II for Commercial Activated Carbon (CA-C), essentially type II for CA-BA-H_3PO_4-40%; the specific surface areas (S_{BET}) are 1560.7401; 1580.6380; 946.7526 ; 722.1510 and 1146.6768 for CA-BA-H_3PO_4-25%, CA-BA-H_3PO_4-40%, CA-C, CA-HT-H_3PO_4-25% and CA-HT-H_3PO_4-40% respectively; For Langmuir, specific surface areas range from CA-HT-H_3PO_4-25% (834.3112 $m^2\ g^{-1}$) < CA-C (1092.9978 $m^2\ g^{-1}$) < CA-HT-H_3PO_4-40% (1325.7948 $m^2\ g^{-1}$) < CA-BA-H_3PO_4-25% (1805.1611 $m^2\ g^{-1}$) < CA-BA-H_3PO_4-40% (1845.6737 $m^2\ g^{-1}$). The three CAEs develop specific surface areas that far exceed the CA-C.

1. Introduction

Activated carbon or activated charcoal (AC) is any carbon which has undergone special preparation and which, as a result, possesses a high degree of property (specific surface area and porosity) to adsorb fluids (gas or liquid) brought into contact with it (Soleimani, 2008; Chen Y et *al.*, 2011; Société

Anonyme de Gestion des Eaux de Paris, 2006; Prakash KBG, et *al.*, 2006). It is an adsorbent material with an amorphous structure composed mainly of carbon atoms, generally obtained after a high-temperature carbonization stage of lignocellulosic biomass, and with a very high specific surface area, giving it a high adsorbent capacity (Société Anonyme de Gestion des Eaux de Paris, 2006; Gueye, 2015; Drissa B et *al.*, 2009; Jean François M, 1995). There are various types of CA with specific surface areas ranging from 100 m^2 g^{-1} to 2,500 m^2 g^{-1}, but the current trend is to use carbons with surface areas ranging from 700 m^2 g^{-1} to 1,800 m^2 g^{-1} (Kiari et *al.*, 2022; Koné et *al.*, 2021; Konan et *al.*, 2020; Ousmaila et *al.*, 2018). It is characterized by its thermostability (Ait S.F, 2011). Today, CA plays an important role in industry, with a wide range of uses, for example in gold extraction, filtration of organic pollutants and water treatment (Siragi et *al.*, 2021). Numerous manufacturing processes (Ousmaila Set *al.*, 2018; Ousmaila, et *al.*, 2016; Maâzou, et *al.*, 2012) have been developed to enable greater production of AC from carbon-rich plant materials such as palm seeds, tamarind wood, husks, coconuts and sugarcane bagasse, with the aim of minimizing production costs and solving the environmental problem associated with their storage in nature (Combere et *al.*, 2017). Niger imports activated carbon, which is used in a variety of fields, despite the country's large reserves of lignocellulosic biomass (Ousmaila, et *al.*, 2016; Maâzou, et *al.*, 2017; Tchakala, et *al.*, 2012; Ousmaila, 2019). These materials end up as waste, which is very difficult for municipalities to manage (Ousmaila, et *al.*, 2016). For this reason, the aim of this work is to determine the specific surface areas of activated carbons produced from the shells of *Balanites aegyptiaca* (L.) Del. and *Hyphaene thebaica* (HT) (L.) Mart. cores by chemical activation with ortho-phosphoric acid (H_3PO_4). This work is part of an extensive research program carried out in our laboratory.

2. Materials and Methods

2.1. Collection and pre-treatment of shells

The shells of the fruits of *Balanites aegyptiaca* (BA) and *Hyphaene Thebaica* (HT) **(Figures 1 and 2)** come from a fruit and vegetable market in the city of Niamey (Niger), called KATAKO. The fruits were first peeled, then the kernels were recovered and crushed by dropping them to separate the shells from the kernels. The shells were then ground in a ball mill. After sieving, the fractions with a diameter between 0.8 and 2 mm were retained for the production of activated carbon and dried in an oven at105°C for 24 hours.

Figure 1. Shells of *Hyphaena thebaica*

Figure 2. Shells of *Balanites aegyptiaca*

2.2. Preparation of activated carbon

This is carried out in three stages (Ousmaila, et *al*., 2016):

- ✓ impregnation of the biomass in solutions of the activating agent;
- ✓ carbonization of the impregnated biomass;
- ✓ purification of the product obtained.

2.2.1. Impregnation

In 250 mL beakers, 16 g of pretreated biomass and 100 mL of activating agent solution (H_3PO_4) were added. The mixture was stirred for 15 hours on a magnetic stirrer **(Figure 3)** at atmospheric pressure and room temperature. The sample was then filtered through ashless filter paper on a Büchner funnel, washed with distilled water, and dried in an oven at 105°C for 24 hours. After removal from the oven, the sample was cooled in a desiccator for 15 minutes.

Figure 3. Impregnation on magnetic stirrers

2.2.2. Pyrolysis

The sample obtained after impregnation was placed in a programmable TACHETE muffle furnace **(Figure 4).** The oven temperature increased up to 450 °C (pyrolysis temperature), with an isothermal plateau of 1h30 min representing the residence time in the oven.

2.2.3. Purification

At the end of the production process, the activated carbon obtained is cooled and then washed thoroughly with hot distilled water to a pH of between 6.5 and 7 to remove impurities **(Figure 5),** then oven-dried at 105 °C for 24 hours.

Figure 4. Muffle furnace

Figure 5. pH meter model HI 991001

2.3. Specific surface areas of activated carbons

The specific surface areas of CAEs are determined. These analyses were carried out at the LABIRIS laboratory of the Université Libre de Bruxelles (ULB) in the Kingdom of Belgium, using a brand-name instrument (MICROMERITICS Gemini VII Surface Area & Porosity) by adsorption of liquid nitrogen at 77 K using the classical Brunauer, Emmet and Teller or BET method. The surface area occupied by one nitrogen molecule is equal to 0.162 nm². The experimental protocol is as follows: the CA was introduced into a BET tube, so as to have a mass of 100 to 130 mg of dry sample. It was treated at 130 °C, under nitrogen flow, for 30 min using a brand-name apparatus (MICROMERITICS FlowPrep 060 Sample Degas System). The sample is then returned to room temperature, still under nitrogen flow. The exact mass of dry sample is determined to the nearest 1/10 mg just before connecting the tube to the BET meter.

2.3.1 Adsorption-desorption isotherms for CAEs

Adsorption-desorption isotherms for N_2 on activated carbon are obtained by plotting the amount of N_2 adsorbed as a function of relative pressure $\frac{P}{P^0}$. The adsorption isotherm covers 50 points over a relative pressure range from 0.01 to 0.99. And the desorption hysteresis covers 15 points over a range of $\frac{P}{P^0}$ from 0.99 to 0.33.

2.3.2. Specific surface areas of CAEs using the BET method

The BET isotherm equation model is used in linear form Eqn. 1. over a range of $\frac{P}{P^0}$ from 0.03 to 0.10 covering 8 points:

$$\frac{P}{q(P^0 - P)} = \left(\frac{C-1}{V_m \times C}\right) \times \frac{P}{P^0} + \frac{1}{V_m \times C} \qquad \textbf{Eqn. 1}$$

The monolayer volume (V_m) and constant C are determined from the slope and y-intercept of the straight line $\frac{P}{q(P^0-P)}$ as a function of $\frac{P}{P^0}$.

Knowing V_m, the SBET specific surface area is determined using equation Eqn. 2.

$$S_{BET} = \sigma . \frac{V_m \times N}{V_M} \qquad \textbf{Eqn. 2}$$

σ being the surface area occupied by an N_2 molecule expressed in nm^2, N the Avogadro number in mol^{-1} and V_M the molar volume in $m^3\ mol^{-1}$.

2.3.3. Specific surface area of CAEs using the Langmuir S_L method

The model is used in form Eqn. 3 over the same relative pressure range as the BET method:

$$\frac{P}{V_{ads}} = \frac{1}{V_m} \times P + \frac{1}{V_m \times b} \qquad \textbf{Eqn. 3}$$

V_m and constant b are determined from the slope and y-intercept of the straight line $\frac{P}{V_{ads}}$ as a function of P.

Knowing V_m, the specific surface area S_L is determined using equation Eqn. 2.

2.3.4. Specific surface area of CAEs according to the Barret Joyner Halenda BJH model

It is determined by the BJH model (on adsorption and desorption) between 17,000 Å and 3,000,000 Å. It is determined using the V_m obtained by discrete analysis of the desorption branch starting from the relative pressure $\frac{P}{P^0}$ of 0.99 to 0.42.

3. Results and Discussion

3.1 Results

Nitrogen (N_2) adsorption isotherms on CAEs

Figure 6 shows the N_2 adsorption-desorption isotherms on the four (4) samples of activated carbons processed (CA-BA-H_3PO_4-25%, CA-BA-H_3PO_4-40%, CA-HT-H_3PO_4-25% and CA-HT-H_3PO_4-40%) and one sample of Commercial Activated Carbon (CA-C).

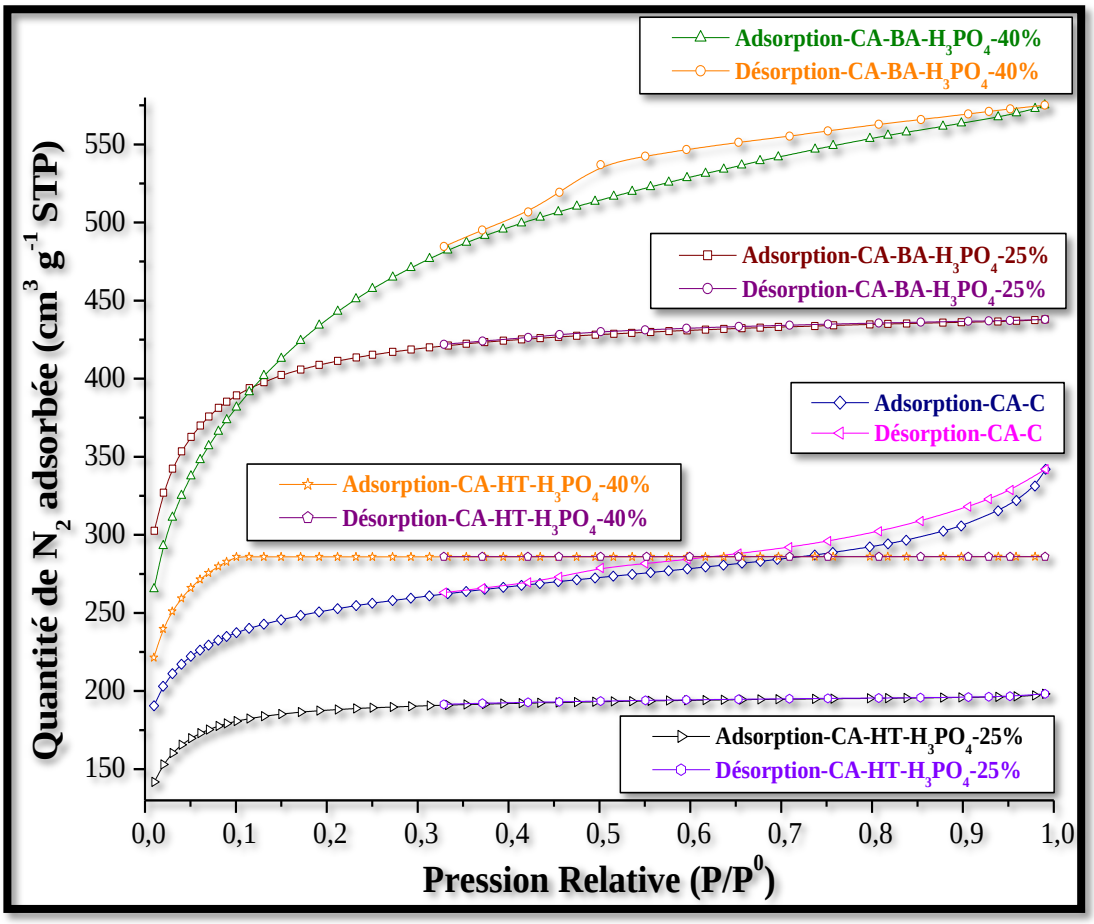

Figure 6. N_2 adsorption isotherms on CAEs and CACs

Initial specific surface areas of single-point P/P_0 CAEs. **Table 1** shows the specific surface areas at the first instant of N_2 adsorption on single-point P/P_0 CAEs.

Table 1. Initial specific surface area at a single P/P_0 point

Ref. Samples	Relative pressure P/P^0	Specific surface ($m^2\ g^{-1}$)
CA-BA-H_3PO_4-25%	0.100805894	1523.7723
CA-BA-H_3PO_4-40%	0.100715366	1494.1115
CAC	0.100593702	929.4722
CA-HT-H_3PO_4-25%	0.100839780	707.4170
CA-HT-H_3PO_4-40%	0.100717811	1119.5753

Specific surface areas of CAEs according to the BET (S_{BET}) model. **Figure 7** shows the N_2 adsorption isotherm models for the five varieties of CAs. The characteristic parameters for linearizing adsorption isotherms using the BET method are shown in **Table 2.** Specific surface areas of CAEs according to the Langmuir S_L model (Galarneau *et al.*, 2018; Aaddouz *et al.*, 2023; Moghadam *et al.*, 2023; Salahat, A. et *al.* 2023; Zerrouk *et al.*, 2025). **Figure 8** shows the N_2 adsorption isotherm models for the five CAE samples. Characteristic parameters for linearization of adsorption isotherms using the Langmuir method are given in **Table 3.**

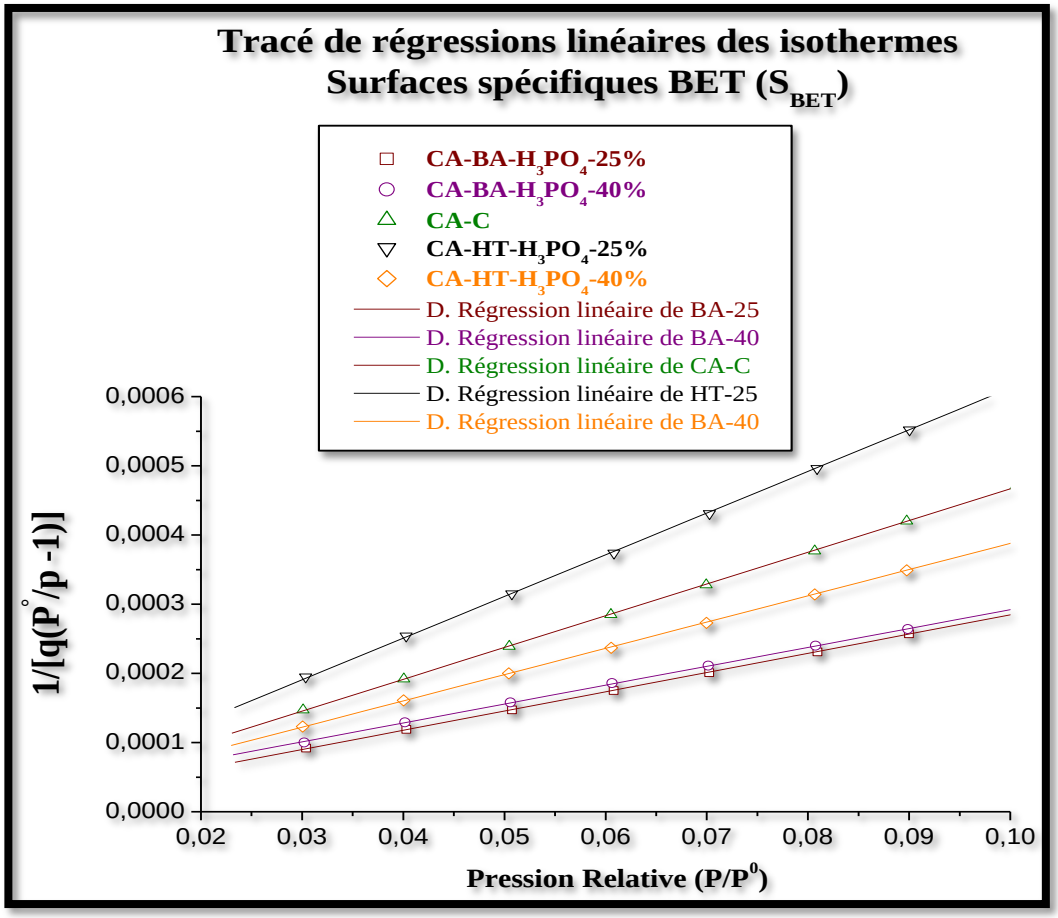

Figure 7. BET linearization of isotherms

Table 2. BET characteristic parameters

Ref. Samples	C	q_{max} ($cm^3\ g^{-1}$ STP)	S_{BET} ($m^2\ g^{-1}$ STP)	R^2
CA-BA-H_3PO_4-25%	440.353856	358.5272	1560.7401±6.1472	0.9999535
CA-BA-H_3PO_4-40%	146.441513	363.0980	1580.6380 ± 7.4106	0.9999335
CA-C	589.936623	217.4844	946.7526 ± 3.2358	0.9999650
CA-HT-H_3PO_4-25%	584.233007	165.8897	722.1510 ± 4.0517	0.9999057
CA-HT-H_3PO_4-40%	431.374623	263.4102	1146.6768 ± 3.9506	0.9999644

Table 3. Langmuir characteristic parameters

Ref. Samples	b ($mmHg^{-1}$)	q_{max} ($cm^3\ g^{-1}$ STP)	S_L ($m^2\ g^{-1}$ STP)	R^2
CA-BA-H_3PO_4-25%	0.181941	414.6746	1805.1611 ± 10.1258	0.999906
CA-BA-H_3PO_4-40%	0.101249	423.9810	1845.6737 ± 26.9855	0.999359
CA-C	0.200744	251.0792	1092.9978 ± 6.5824	0.999891
CA-HT-H_3PO_4-25%	0.199634	191.6547	834.3112 ± 3.2107	0.999956
CA-HT-H_3PO_4-40%	0.178439	304.5564	1325.7948 ± 8.1655	0.999886

Specific surface areas of CAEs using the BJH (S_{BJH}) model

The cumulative specific surface areas of pores using the BJH method are shown in **Table 4.**

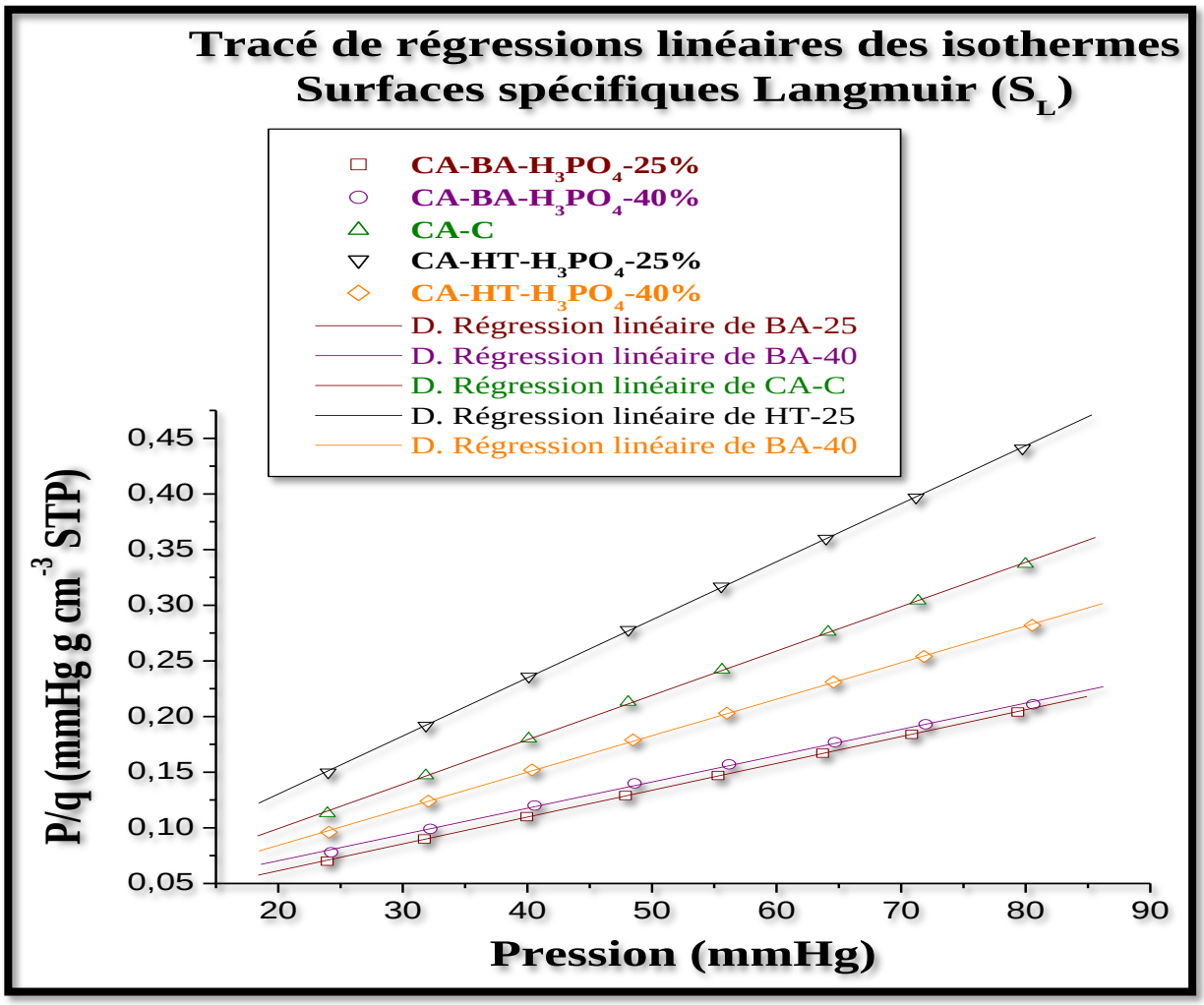

Figure 8. Linearization of Langmuir isotherms

Table 4. Cumulative specific surface area BJH

Ref. Samples	Cumulative specific surface area ($m^2\ g^{-1}$)	
	Adsorption	Desorption
CA-BA-H_3PO_4-25%	996.321	43.6906
CA-BA-H_3PO_4-40%	829.192	251.5097
CA-C	283.921	98.8477
CA-HT-H_3PO_4-25%	543.029	12.4854
CA-HT-H_3PO_4-40%	744.577	35.9795

Table 5 shows the comparison of the BET Surfaces of CAEs with those of the literature.

Table 5. Comparison of the S_{BET} of CAEs with those of the literature

Biomass	Activation	S_{BET} (m^2/g)	References
CA-BA-H_3PO_4-25%	H_3PO_4	1560.7401±6.1472	[This work]
CA-BA-H_3PO_4-40%	H_3PO_4	158.6380 ± 7.4106	[This work]
CA-C	H_3PO_4	946.7526 ± 3.2358	[This work]
CA-HT-H_3PO_4-25%	H_3PO_4	722.1510 ± 4.0517	[This work]
CA-HT-H_3PO_4-40%	H_3PO_4	1146.6768 ± 3.9506	[This work]
Peanut shells	KOH	751	(Gueye. 2015)
Bagasse	H_3PO_4	750	(Stoeckli, H. F. 1990)
Rice straw	H_3PO_4	674	(Stoeckli, H. F. 1990)
Coconut	H_3PO_4	746	(Gueye. 2015)
Eucalyptus wood	H_3PO_4	500-1239	(Reddad Z. 2002).
Shea cake	H_3PO_4	1148	(Tchakala I. et *al.* 2012)
Rice straw	(KOH)	370-2410	(Wang, Z. et *al.* 2011)
Cotton cake	H_3PO_4	584	(Tchakala I. et *al.* 2012)
Biochar	KOH	-	(Ould-Idriss, A. et *al.* 2011),
Olive pits	H_3PO_4	700-1050	(Puziy, A. et *al.* 2007)
Desert plants	$ZnCl_2$	-	(Daud et *al.* 2004)
Jatropha wood	H_3PO_4	1305	(Gueye. 2015)
Jatropha shells	H_3PO_4	364	(Gueye, 2015)
Peach pits	H_3PO_4	1112-1393	(Seredych, M. et *al.* 2009)
Artichoke leaves	(KOH)	753-2038	(Chingombe, P., et *al.* 2005)
Coconut	H_3PO_4	1300	(Phan, N. H., et *al.* 2006)
Olive pits	H_3PO_4	1700	(Yavuz, R., et *al.* 2010)
Pine wood	H_3PO_4	1400	(Hared, H. I., et *al.* 2007)
Palm shells	H_3PO_4	380	(Arami-Niya, A., et al. 2011)
Date pits		1400	(Girgis, B. S.et *al.* 2002)
Olive waste	KOH	1750	(Moreno-Castilla, et *al.* 2001)
Palm stems	KOH	950	(Jibril, B., et *al.* 2008)
Corn cobs	KOH	1400	(Bagheri, N.et *al.* 2009)
Pistachio shells	KOH	800	(Lua, A.C.et *al.* 2004)
Coconut	KOH	291.74- 665.79	(Drissa, B., et *al.* 2009)

3.2 . Discussion

Analysis of the results presented in Figure 6 and Table 1 show that:

- ✓ the adsorption isotherms of CA-BA-H_3PO_4-25%, CA-HT-H_3PO_4-25% and CA-HT-H_3PO_4-40% show a high adsorption capacity (rapid growth with 1523.7723; 707.4170 and 1119.5753 $m^2\ g^{-1}$ respectively) of N_2 at very low relative pressures ($P/P^0 \cong 0.100$) and then a plateau reflecting saturation of these CAs, despite the increase in relative pressure. They are concave towards the relative pressure axis. The adsorption-desorption curves obtained do not exhibit hysteresis. The desorption branches join the adsorption branches at relative pressures above 0.32 **(Figure 6).** These characteristics are essentially indicative of the majority distribution of micropores. The adsorption isotherms obtained in this case are essentially type I according to the BDDT classification. The rapid rise results from increased CAs-N_2 interactions in the micropores. This could be interpreted as equivalent adsorption sites, with micropores predominating;

- ✓ in the case of CA-C, the isotherm also shows strong N_2 adsorption (929.4722 m^2 g^{-1}) at very low relative pressure (P/P^0 =0.100593702). This is characteristic of micropore filling (type I). However, a relatively gradual increase in the amount of N_2 adsorbed is observed. Indeed, the adsorption-desorption curve obtained shows a slight hysteresis. The desorption branch does not join the adsorption branch at all for a relative pressure greater than 0.32 (**Figure 6**). This hysteresis is indicative of the presence of stable mesopores. Pore saturation appears to occur at the highest relative pressure (inflection of the adsorption curve). These characterize the filling of the external surface of the CAC. The adsorption isotherm obtained in this case is of mixed type II, resulting from a sum of I + II isotherms (filling of micropores followed by multilayer adsorption on an external surface of similar proportion) according to the BDDT classification (Ousmaila, 2019);
- ✓ on the other hand, in the case of CA-BA-H_3PO_4-40%, there is a strong adsorption (1494.1115 m^2 g_{-1}) followed by a very gradual increase in the amount of N_2 adsorbed as a function of relative pressure. The resulting adsorption-desorption curve exhibits hysteresis. The desorption branch does not join the adsorption branch at relative pressures above 0.32 (Figure 6). This adsorption isotherm obtained is essentially attributable to type II according to the BDDT classification, and the hysteresis would be similar to type A according to the DeBoer classification. CA-BA-H_3PO_4-40% contains tubular pore size distributions of varying widths (micropores and mesopores). It has a continuous transition from monolayer and multilayer adsorption to capillary condensation;
- ✓ Specific surface areas at the single low relative pressure range as follows: CA-HT-$_{H3PO4}$-25% < CA-C < CA-HT-H_3PO_4-40% < CA-BA-H_3PO_4-40% < CA-BA-H_3PO_4-25% (**Table 1**).

BET modeling results (Figure 7 and Table 2) show that:

- ✓ the R^2 correlation coefficients obtained are highly significant and very close to unity (Table 2). They are of the order of 0.9999535; 0.9999335; 0.9999650; 0.9999057 and 0.9999644 for CA-BA-H_3PO_4-25%; CA-BA-H_3PO_4-40%; CA-C; CA-HT-H_3PO_4-25% and CA-HT-H_3PO_4-40% respectively (Figure 7 and Table 2). This indicates that CA-C fits this model better than the others. They then range to CA-HT-H_3PO_4-40% <CA-BA-H_3PO_4-25% < CA-BA-H_3PO_4-40% < CA-HT-H_3PO_4-25%;
- ✓ N_2-CAs characteristic constants (C) range from 146.441513 to 589.936623 for CA-BA-H_3PO4-40% and CA-C respectively. They are well in excess of 1. This implies that the heat of adsorption (Eads) of N_2-CAs is greater than that of liquefaction (Eliq). In this case, there would be much more adsorption than liquefaction. As a result, the type III isotherm would not have been observed. C values range from CA-BA-H_3PO_4-40% (146.441513) < CA-HT-H_3PO_4-40% (431.374623) < CA-BA-H_3PO_4-25% (440.353856) < CA-HT-H_3PO_4-25% (584.233007) < CA-C (589.936623);
- ✓ N_2-CAs adsorption maxima range from 165.8897 to 363.0980 cm^3 g^{-1} for CA-HT-H_3PO_4-25% and CA-BA-H_3PO_4-40% respectively. Excluding these samples, they range as follows: CA-C (217.4844 cm^3 g^{-1}) < CA-HT-H_3PO_4-40% (263.4102 cm^3 g^{-1}) < CA-HT-H_3PO_4-25% (358.5272 cm^3 g^{-1}). These indicate that, with the exception of CA-HT-H_3PO_4-25%, all three CAEs have developed adsorption capacities that far exceed CA-C. Moreover, as the concentration of the activating agent increases, so do the adsorption capacities;

- ✓ specific surface area increases with the concentration of activating agent, whatever the biomass used. The best specific surface is obtained at 40%. The specific surface areas of BA samples exceed those of HT samples. This would indicate that BA is the best biomass for the elaboration of CAs. The calculated specific surface areas (SBET) are 1560.7401; 1580.6380; 946.7526; 722.1510 and 1146.6768 $m^2 g^{-1}$ for CA-BA-H_3PO_4-25%, CA-BA-H_3PO_4-40%, CA-C, CA-HT-H_3PO_4-25% and CA-HT-H_3PO_4-40% respectively. In addition, CA-BA-H_3PO_4-25% and CA-BA-H_3PO_4-40% were reported to have specific surface areas almost double that of CA-C. This shows that all three CAEs have developed specific surface areas that far exceed those of CA-C, suggesting that these samples would be good adsorbents for industrial applications such as wastewater treatment for effluent retention, ore processing for gold and silver extraction, and so on.

The Langmuir modeling results (Figure 8 and Table 3) show that:

- ✓ the correlation coefficients (R^2) obtained are highly significant and very close to unity. They are of the order of 0.999906; 0.999359; 0.999891; 0.999956 and 0.999886 respectively for CA-BA-H_3PO_4-25%; CA-BA-H_3PO_4-40%; CA-C; CA-HT-H_3PO_4-25% and CA-HT-H_3PO_4-40% (Table 3). This indicates that CA-HT-H_3PO_4-25% fits this model better than the others. They then range to CA-BA-H_3PO_4-25% < CA-C < CA-HT-H_3PO_4-40% < CA-BA-H_3PO_4-40% ;
- ✓ Langmuir constants for N_2-CAs (b) range from 0.101249 to 0.200744 $mmHg^{-1}$ for CA-BA-H_3PO_4-40% and CA-C respectively. This is in agreement with the BET constants (C). All these values lie between 0 and 1, suggesting that the N_2-CAs adsorption process is more favorable, and that the heat of desorption is greater than that of adsorption. Except for BA-H_3PO_4-40% and CA-C; constants (b) range from CA-HT-H_3PO_4-40% (0.178439 $mmHg^{-1}$) < CA-BA-H_3PO_4-25% (0.181941 $mmHg^{-1}$) < CA-HT-H_3PO_4-25% (0.199634 $mmHg^{-1}$). Adsorption is most favored for CA-C followed by CA-HT-H_3PO_4-25% ;
- ✓ N_2-CAs adsorption maxima range from 191.6547 to 423.9810 $cm^3 g^{-1}$ for CA-HT-H_3PO_4-25% and CA-BA-H_3PO_4-40% respectively. Excluding these samples, they range as follows: CA-C (251.0792 $cm^3 g^{-1}$) < CA-HT-H_3PO_4-40% (304.5564 $cm^3 g^{-1}$) < CA-BA-H_3PO_4-25% (414.6746 $cm^3 g^{-1}$). This would indicate that, apart from CA-HT-H_3PO_4-25%, all three CAEs have developed Langmuir adsorption capacities that far exceed CA-C. What's more, as the concentration of activating agent increases, so do the adsorption capacities. These are in line with the maximum amounts of M-BET;
- ✓ the calculated specific surface areas (S_L) are much higher than those of BET. They range from 834.3112 to 1845.6737 $m^2 g^{-1}$ for CA-HT-H_3PO_4-25% and CA-BA-H_3PO_4-40%. They then follow as follows for CA-C (1092.9978 $m^2 g^{-1}$) < CA-HT-H_3PO_4-40% (1325.7948 $m^2 g^{-1}$) < CA-BA-H_3PO_4-25% (1805.1611 $m^2 g^{-1}$). The surface area also increases with the percentage of activating agent, as in the case of S_{BET}. The best specific surface area is obtained at 40%. The specific surface areas of the BA samples exceed those of the HT samples. This indicates that BA is the best biomass for the elaboration of CAs. In addition, CA-BA-H_3PO_4-25% and CA-BA-H_3PO_4-40% have specific surface areas almost double that of CA-C. This shows that the three CAEs develop specific surface areas that far exceed CA-C. These confirm all the S_{BET} results.

Analysis of the results presented in Table 4 shows that:

- ✓ adsorption: the calculated cumulative specific surface areas (S_{BJH}) are lower than those of S_{BET} and S_L. They range from 283.921 to 996.321 $m^2 g^{-1}$ for CA-C and CA-BA-H^3PO^4-25%. Then, they follow as follows for CA-HT-H_3PO_4-25% (543.029 $m^2 g^{-1}$) < CA-HT-H_3PO_4-40% (744.577 $m^2 g^{-1}$) < CA-BA-H_3PO_4-40% (829.192 $m^2 g^{-1}$). The surface area increases with the percentage of activating agent in the case of HT, but decreases in the case of BA. Thus, the best specific surface area is obtained at 25%. The specific surface areas of all CAEs exceed those of the CA-C sample. This confirms that BA is the best biomass for the elaboration of CAs.
- ✓ for desorption, S_{BJHs} vary from 12.4854 to 251.5097 $m^2 g^{-1}$ for CA-HT-H_3PO_4-25% and CA-BA-H_3PO_4-40%. They then follow as follows for CA-HT-H_3PO_4-40% (35.9795 $m^2 g^{-1}$) < CA-BA-H_3PO_4-25% (43.6906 $m^2 g^{-1}$) < CA-BA-H_3PO_4-40% (98.8477 $m^2 g^{-1}$). The surface area increases with the percentage of activating agent for BA and HT. Thus, the best specific surface area is obtained at 40% for BA. This confirms that BA is the best biomass.

4. Conclusion

These studies show that :

- ✓ the N_2 adsorption isotherms are essentially attributable to type I (according to BDDT) for CA-BA-H_3PO_4-25%, CA-HT-H_3PO_4-25% and CA-HT-H_3PO_4-40%;
- ✓ the CA-C adsorption isotherm is attributable to mixed type II;
- ✓ the CA-BA-H_3PO_4-40% isotherm is mainly attributable to type II;
- ✓ the hysteresis is similar to type A;
- ✓ the calculated specific surface areas (S_{BET}) are of the order of 1560.7401; 1580.6380; 946.7526; 722.1510 and 1146.6768 for CA-BA-H_3PO_4-25%, CA-BA-H_3PO_4-40%, CA-C, CA-HT-H_3PO_4-25% and CA-HT-H_3PO_4-40% respectively;
- ✓ specific surface areas according to the Langmuir model range from CA-HT-H_3PO_4-25% (834.3112 $m^2 g^{-1}$) < CA-C (1092.9978 $m^2 g^{-1}$) < CA-HT-H_3PO_4-40% (1325.7948 $m^2 g^{-1}$) < CA-BA-H^3PO^4-25% (1805.1611 $m^2 g^{-1}$) < CA-BA-H_3PO_4-40% (1845.6737 $m^2 g^{-1}$) ;
- ✓ CA-BA-H_3PO_4-25% and CA-BA-H_3PO_4-40% have specific surface areas almost double those of CA-C;
- ✓ The three CAEs develop specific surface areas well in excess of CA-C.

References

Aaddouz M., Azzaoui K., Akartasse N., Mejdoubi E., Hammouti B., Taleb M., Sabbahi R., Alshahateet S.F. (2023). Removal of Methylene Blue from aqueous solution by adsorption onto hydroxyapatite nanoparticles, *Journal of Molecular Structure*, 1288, 135807, https://doi.org/10.1016/j.molstruc.2023.135807

Ait, S. F. (2011) Adsorption of phenol by a mixture of adsorbents (bentonite - activated carbon). Magister at the University of Boumerdèz UB, Boumerdèz-Algeria BA, 2011, 106.

Arami-Niya, A., Daud, W.M.A.W. & Mjalli, F. S. (2011) Comparative study of the textural characteristics of oil palm shell activated carbon produced by chemical and physical activation for methane adsorption, *Chemical Engineering Research and Design*, 89 (6), 657-664. https://doi.org/10.1016/j.cherd.2010.10.003

Bagheri, N. & Abedi, J. (2009) Preparation of high surface area activated carbon from corn by chemical activation using potassium hydroxide, *Chemical Engineering Research and Design*, 87 (8) 1059-1064. DOI : https://doi.org/10.1016/j.cherd.2009.02.001

Chen Y. et *al*. (2011) Application studies of carbon derived from rice husks produced by chemical-thermal process. A review, *Adv. Colloïd interface Sci* 163, 39-52.

Chingombe P., Saha B., Wakeman R.J. (2005) Surface modification and characterisation of a coal-based activated carbon, *Carbon*, 43 (15) 3132-3143. https://doi.org/10.1016/j.carbon.2005.06.021

Combere W, Arsene H. Y, Abdoulaye D, Kabore L. (2017) Elimination du chrome trivalent des eaux par des zéolithes échangées au fer et des argiles naturelles du Burkina Faso. *J. Soc. West-Afr. Chem.*, 043, 26 – 30.

Daud, W. M. A. W. & Ali, W. S.W. (2004) Comparison on pore development of activated carbon produced from palm shell and coconut shell, *Bioresour Technol*, 93 (1) 63-69. https://doi.org/10.1016/j.biortech.2003.09.015

Drissa B et *al*. (2009) Etude comparée des méthodes de production de charbon actif, suivie d'un test de dépollution d'une eau contaminée au diuron. *J. Soc. Ouest-Afr. Chim* 28, 41-52.

Drissa, B., Bini, D., Albert, T., Guessan, E. Z., Grah, P. A., Didier, R., & Jean, V. W. (2009) Etudes comparées des méthodes de préparation du charbon actif, suivie d'un test de dépollution d'une eau contaminée au Diuron, *J. Soc. Ouest-Afr. Chim.* 028, 41-52.

Galarneau A., Mehlhorn D., Guenneau F., Coasne B., Villemot F., Minoux D., Aquino C., Dath J-P. (2018). Specific Surface Area Determination for Microporous/Mesoporous Materials: The Case of Mesoporous FAU-Y Zeolites, *Langmuir*, 34 (47), 14134-14142 https://doi.org/10.1021/acs.langmuir.8b02144

Girgis, B. S. & El-Hendawy, A. (2002) Porositydevelopment in activated carbons obtained from datepits under chemical activation with phosphoric acid, *Microporous Mesoporous meter*, 52, 105-117.

Gueye, M. (2015) Development of activated carbon from lignocellulosic biomass for applications in water treatment. Doctoral thesis at the International Institute for Water and the Environment (2iE), Ouagadougou/Burkina Faso OBF, 215.

Hared, H. I., Dirion, J-L., Salvador, S., Lacroix, M. & Rio, S. (2007) Pyrolysis of wood impregnated with phosphoric acid for the production of activated carbon: Kinetics and porosity development studies, *Journal of Analytical and Applied Pyrolysis*, 79 (1–2) 101-105. https://doi.org/10.1016/j.jaap.2006.12.016

Jean François M. (1995) Fabrication et caractérisation d'un charbon actif rustique issu de la biomasse. Université de Technologie de Compiègne – option Génie des Procédés Industriels 96, 29-32.

Jibril, B., Houache, O., Al-Maamari, R. & Al-Rashidi, B. (2008) Effects of H_3PO_4 and KOH in carbonization of lignocellulosic material, *Journal of Analytical and Applied Pyrolysis*, 83 (2) 151-156. https://doi.org/10.1016/j.jaap.2008.07.003

Kiari, M.N.A., Fanou, G.D., Sylvie, A.T., Ouattara, A., Kone, H., Alma, M.M.M., Assidjo, E.N., Yao, K.B. (2022) Process conditions optimization of plant waste-derived microporous activated carbon using a full factorial design and genetic algorithm, *Journal of Materials and Environmental Science*, Volume 13, Issue 8, 884-899.

Konan, A.T.S., Richard, R., Andriantsiferana, C., Yao, K.B. (2020) Recovery of borassus palm tree and bamboo waste into activated carbon: application to the phenolic compound removal. *Journal of Materials and Environmental Science*, Volume 11, Issue 10, 1584-1598.

Koné, H., Kouassi, K.E., Assémian, A.S., Yao, K.B., Drogui, P. (2021) Investigation of breakthrough point variation using a semi-industrial prototype packed with low-cost activated carbon for water purification. *Journal of Materials and Environmental Science*, Volume 12, Issue 02, 224-243.

Lua, A.C. & Yang, T. (2004) Effect of activation temperature on the textural and chemical properties of potassium hydroxide activated carbon prepared from pistachio-nut shell : *Journal of Colloid and Interface Science*, 274 (2) 594-601. https://doi.org/10.1016/j.jcis.2003.10.001

Maâzou, S.D.B., Hima, I. H., Maman Mousbahou, M. A., Adamou, Z., Ibrahim, N. (2017) Elimination du chrome par du charbon actif élaboré et caractérisé à partir de la coque du noyau de Balanites agyptiaca : *Int. J. Biol. Chem. Sci.*, 11(6), 3050-3065. https://dx.doi.org/10.4314/ijbcs.v11i6.39

Moghadam R.P., Shukla C.A., Ranade V.V. (2023). Novel Machine Learning-Based Method for Estimation of the Surface Area of Porous Silica Particles. *Ind Eng Chem Res.* 62(44), 18810-18821. https://doi.org/10.1021/acs.iecr.3c02785

Moreno-Castilla, C., Carrasco-Marín, F., López-Ramón, M. V. & Alvarez-Merino, M. A. (2001) Chemical and physical activation of olive-mill waste water to produce activated carbons, *Carbon*, 39 (9) 1415-1420. https://doi.org/10.1016/S0008-6223(00)00268-2

Ould-Idriss, A., Stitou, M., Cuerda-Correa, E. M., Fernández-González, C., Macías-García, A., Alexandre-Franco, M. F., Gómez-Serrano, V. (2011) Preparation of activated carbons from olive-tree wood revisited. II. Physical activation with air, *Fuel Processing Technology*, 92 (2) 266-270. https://doi.org/10.1016/j.fuproc.2010.05.018

Ousmaila S M, Maâzou S.B. D, Abdoul Rachid C. Y, Maman Mousbahou M. A, Ibrahim N. (2018) Valorization of Balanites aegyptiaca *(L.) Del*. nut shells. and elimination of chromium in solution. *Afrique SCIENCE*, 14 (3), 167 – 181.

Ousmaila S.M, Maˆazou S.D.B, Mousbahou M.A.M, Ibrahim N. (2018) Valorisation des coques de noyaux de Balanites aegyptiaca *(L.) Del.* et Hyphaene th´ebaica *(L.) Mart*, pour l'´elaboration et caracterisation de Charbons Actifs; application pour l'elimination du chrome. *ESJ* 14 195, https://doi.org/10.19044/esj.2018.v14n21p195

Ousmaila, S.M., Adamou, Z., Ibrahim, D., & Ibrahim, N. (2016) Préparation et caractérisation de charbons actifs à base de coques de noyaux de Balanites eagyptiaca et de Zizyphus mauritiana : *J. Soc. Ouest-Afr. Chim.* 041, 59- 67.

Ousmaila, SM. (2019) Valorization of agro-food wastes for the elaboration of activated carbons; characterization and application in the depollution of wastewater loaded with chromium from the Malam Yaro Tannery of Zinder-Niger. [Doctoral thesis]. Abdou Moumouni University of Niamey. These of Doctorate Chemistry of Metals.

Phan, N. H., Rio, S., Faur, C., Coq, L. L., Cloirec, P. L. & Nguyen, T. H. (2006) Production of fibrous activated carbons from natural cellulose (jute, coconut) fibers for water treatment applications. *Carbon*, 44 (12) 2569-2577. https://doi.org/10.1016/j.carbon.2006.05.048

Prakash KBG, shivakami K, Miranda LR, Velan M. (2006) Preparation of steam activated carbon from Rubberwood sawdust (Hevea brasiliensis) and its adsorption kinetics. *J. Hazard. Matter. B* 136, 133-142.

Puziy, A. M., Poddubnaya, O. I., Martínez-Alonso, A., Castro-Muñiz, A., Suárez-García, F. & Tascón, J. M. D. (2007) Oxygen and phosphorus enriched carbons from lignocellulosic material : *Carbon*, 45 (10) 1941-1950. https://doi.org/10.1016/j.carbon.2007.06.014

Reddad, Z. (2002) Procédés d'élimination des ions métalliques par adsorption sur un polysaccharide naturel - Etude expérimentale et modélisation. Thèse de doctorat à l'Université de Nantes UN, Nantes-France NF, 288.

Salahat, A., Hamed, O., Deghles, A., Azzaoui, K., Qrareya, H., Assali, M., Mansour, W., Jodeh, S., Hacıosmanoğlu, G.G., Can, Z.S., Hammouti, B., Nandiyanto, A.B.D., Ayerdi-Gotor, A., Rhazi, L. (2023). Olive Industry Solid Waste-Based Biosorbent: Synthesis and Application in Wastewater Purification. *Polymers*, 15, 797. https://doi.org/10.3390/polym15040797

Seredych, M. & Bandosz, T. J. (2009) Adsorption of hydrogen sulfide on graphite derived materials modified by incorporation of nitrogen, *Materials Chemistry and Physics*, 113 (2) 946-952. https://doi.org/10.1016/j.matchemphys.2008.08.073

Siragi D. B M, Desmecht D, Hima H. I, Mamane O. S, Natatou I. (2021) Optimization of Activated Carbons Prepared from <i>Parinari macrophylla</i> Shells. *MSA*, 12, no 05, p. 207-222, doi: 10.4236/msa.2021.125014.

Société Anonyme de Gestion des Eaux de Paris. (2006) Traitement de potabilisation des eaux de surface, adsorption sur charbon actif. Conf.

Soleimani M, Kaghazchi T. (2008) Adsorption of gold ions from industrial wastewater using activated carbon derived from hard shell of apricot stones. An agricultural waste. *Bioresourtechno* 99, 5374-5383.

Stoeckli, H. F. (1990) Microporous carbons and their characterization: The present state of the art : *Carbon*, 28 (1) 1-6. https://doi.org/10.1016/0008-6223(90)90086-E

Tchakala, I., Bawa, L. M., Djaneye-Boundjou, G., Doni, K.S., Nambo, P. (2012) Optimisation du procédé de préparation des charbons actifs par voie chimique (H_3PO_4) à partir des tourteaux de Karité et des tourteaux de Coton : *Int. J. Biol. Chem. Sci.* 6 (1), 461–478. http://dx.doi.org/10.4314/ijbcs.v6i1.42

Wang, Z., Nie, E., Li, J., Zhao, Y., Luo, X. & Zheng, Z. (2011) Carbons prepared from Spartina alterniflora and its anaerobically digested residue by H_3PO_4 activation: Characterization and adsorption of cadmium from aqueous solutions : *Journal of Hazardous Materials*, 188 (1–3) 29-36. https://doi.org/10.1016/j.jhazmat.2011.01.041

Yavuz, R., Akyildiz, H., Karatepe, N. & Çetinkaya, E. (2010) Influence of preparation conditions on porous structures of olive stone activated by H_3PO_4, *Fuel Processing Technology*, 91 (1) 80-87. https://doi.org/10.1016/j.fuproc.2009.08.018

Zerrouk M., Er-rajy M., Azzaoui K., Sabbahi R., Hanbali G., Jodeh S., Alshahateet S.F., Hammouti B., Kaya S., Maslov M. M., Lachkar M., Ouarsal R. (2025). DFT Computation-Assisted Design and synthesis of trisodium nickel triphosphate: Crystal Structure, Vibrational study, DFT Computation, Electronic Properties and Application in Wastewater Purification, *Journal of Molecular Structure*, 141450, https://doi.org/10.1016/j.molstruc.2025.141450